DIRECT NUMERICAL SIMULATION OF THE GROWTH OF COHERENT FLOW STRUCTURES IN A TRIGGERED TURBULENT SPOT

Joshua R. Brinkerhoff
Department of Mechanical and Aerospace Engineering
Carleton University
1125 Colonel By Drive, Ottawa, Canada, K1S 5B6

Metin I. Yaras
Department of Mechanical and Aerospace Engineering
Carleton University
1125 Colonel By Drive, Ottawa, Canada, K1S 5B6
metin_yaras@carleton.ca

ABSTRACT

Hairpin-like coherent flow structures have been identified as the dominant vortical structures in transitional and turbulent boundary layers and free shear layers. To fully characterize the processes occurring within such flows, it is important to study the growth mechanism of the hairpin vortices, particularly at their early stages of development, and the development of the resultant wave packets containing multiples of these flow structures. The formation of an artificially-triggered turbulent spot in isolation provides a suitable test case to study the mechanism through which a hairpin vortex forms in a shear layer and how the formation of one such flow structure may produce a local flow environment that promotes the creation of similar flow structures in sequence. The present study involves direct numerical simulations wherein an isolated turbulent spot is produced through a perturbation in the form of a pulsed jet ejected transversely through a square orifice in the test surface. The simulated spots compare favorably with spots measured experimentally under similar freestream conditions. Two levels of freestream acceleration—one that is nominally zero and another that is above the typical threshold required for relaminarization—are applied to the flow to assess the sensitivity of the hairpin-like vortical structures to freestream acceleration. Hairpin-like vortices near the spot trailing edge are observed to grow primarily through an instability of shear layers created between high- and low-velocity streaks near the spanwise edges of the spot.

INTRODUCTION

A turbulent spot is a localized region of turbulent flow within a laminar shear layer that may develop naturally through the non-linear growth of Tollmien-Schlichting waves, as in the early observations of turbulent spots by Emmons (1951), or be triggered artificially using (among other things) electric sparks (Wygnanski et al., 1976), localized roughness elements (Chong and Zhong, 2003), or intermittent wall jets (Perry et al., 1981). The amplification of disturbances leads to the formation of three-dimensional vortical structures that initiate higher instability modes that sustain the turbulence and lead to the spatial growth of the turbulent region. Numerous flow visualization experiments (e.g. Gad-El-Hak et al., 1981), hot-wire and particle-image-velocimetry measurements (e.g. Makita and Nishizawa, 2001; Schröder and Kompenhans, 2004; Yaras, 2007), and direct numerical simulations (e.g. Singer, 1996; Strand and Goldstein, 2011) have identified that the dominant coherent flow structures in the spot are streamwise-elongated, hairpin-like vortices, and the growth of these vortices provide the principal mechanism for the spatial development of the turbulent spot (e.g. Schröder et al., 2008).

Considering the important role that hairpin vortices play in the development of a turbulent spot, understanding the mechanism by which these flow structures are created and grow is an important step in characterizing the development of the spot. Through direct numerical simulation, Singer and Joslin (1994) observed that ejection of low-momentum fluid between the legs of an artificially-triggered hairpin vortex creates transient regions of locally-adverse pressure gradient, resulting in unsteady separation of flow near the wall. Separation occurs primarily in the spanwise/wall-normal plane and the unsteady separated shear layer rolls-up into streamwise-oriented vortices. A similar mechanism in the streamwise/wall-normal plane produces the spanwise-oriented heads of the hairpin vortices. The above mechanisms are qualitatively confirmed by visualization experiments of Guo et al. (2004) and the vortex-regeneration model of Smith et al. (1991) that is based on complementary experimental and computational studies of fully-turbulent boundary layers. However, tomagraphic particle-image-velocimetry experiments of triggered turbulent spots by Schröder and Kompenhans (2004) and Schröder et al. (2008) suggest an alternative mechanism for the development of secondary flow structures

from an initial hairpin vortex. Their results show that a shear layer is created between the high- and low-velocity streamwise streaks that are formed by the upwash and downwash velocities induced by the hairpin vortex, and an instability of this shear layer through an inviscid instability mode in the streamwise/spanwise plane leads to streamwise grouping of wall-normal vorticity. The wall-normal vortices are unstable and quickly fold over into arch-shaped structures that are then stretched by the mean shear to form hairpin vortices.

The hairpin-vortex regeneration mechanism proposed by Singer and Joslin (1994) suggests that a secondary hairpin vortex will develop between the legs of a primary hairpin vortex, while the mechanism proposed by Schröder and Kompenhans (2004) suggests that a secondary hairpin vortex will straddle a leg of the primary hairpin vortex. Published literature contains instances of turbulent spots with both kinds of hairpin-vortex topology, and it is not clear what flow conditions produce a more favorable environment for one mechanism to occur over the other. Therefore, the present study involves direct numerical simulations wherein an isolated turbulent spot is produced through a perturbation in the form of a pulsed jet ejected transversely through a square orifice in the test surface, and the results are analyzed to provide further insight into the growth mechanisms of the coherent flow structures within the spot. Two cases—one with non-accelerating and the other with strongly-accelerating freestream conditions—are simulated to assess the sensitivity of the development of coherent flow structures within the spot to freestream acceleration.

NUMERICAL METHOD

The computational domain, shown in Figure 1, consists of a main-flow sub-domain containing a flat, no-slip test surface and a jet sub-domain comprised of a rectangular pipe. The main-flow sub-domain has streamwise and spanwise dimensions of L = 550 mm and 0.20L, respectively, and the square jet sub-domain has dimensions of D = 2.2 mm and a wall-normal length of 10D. The wall-normal height of the main-flow sub-domain at the leading edge is 0.42L. A uniform, time-invariant velocity of U_0 = 4 m/s parallel to the test surface and a static pressure that remains fixed in an area-averaged sense are specified at the inflow and outflow boundaries of the main-flow sub-domain, respectively, and the sides and upper wall are specified as free-slip walls. The level of freestream acceleration is adjusted by sloping the upper wall at a constant angle; the inclination angles for the non-accelerating and accelerating cases are shown in Table 1. Turbulent spots are artificially triggered by impulsively ejecting a stream of high-velocity fluid from the jet sub-domain into the laminar boundary layer that develops on the test surface. The centerline of the jet orifice is located at the midspan of the test surface and 0.325L from the test-surface leading edge. The sides of the jet sub-domain are specified as no-slip walls to allow development of the boundary layer within the jet pipe. A spatially-uniform velocity of 35 m/s is applied at the inlet of the jet sub-domain for a duration of t_{jet} = 8.65 ms. Growth of the jet boundary layer along the walls of the jet sub-domain accelerates the core flow in the jet to a value of v_{jet} = 44 m/s at the center of the jet orifice.

A structured grid consisting of hexahedral finite volumes

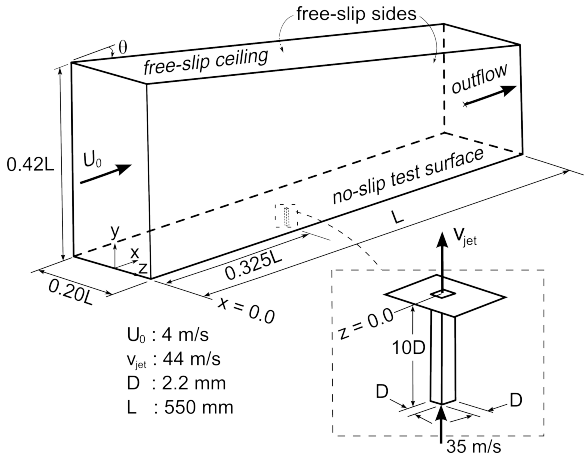

Figure 1. Schematic of the computational domain. A magnified view of the jet sub-domain is shown in the dashed box.

was mapped to the test-surface and jet sub-domains described above. The test-surface sub-domain is discretized with 345, 88, and 197 nodes in the streamwise, wall-normal, and spanwise directions, respectively. The nodes are distributed so that the average streamwise and spanwise spacing within the triggered turbulent spot is $\Delta x^+ = 28$ and $\Delta z^+ = 11$, respectively. Nodes are distributed in the wall-normal direction to place the first node from the no-slip boundary at $y^+ = 0.91$ and nine nodes below $y^+ = 10$. In the jet sub-domain, the directions normal to the jet flow (x and z) are discretized with 60 nodes, spaced to place at least 20 nodes in the jet boundary layer, while the direction parallel to the jet flow is discretized with 88 nodes that are distributed to provide the highest spatial resolution near the jet orifice.

ANSYS CFX ® (Version 12), a commercial computational fluid dynamics software package, was used to solve the incompressible form of the time-varying mass- and momentum-conservation equations through a finite-volume approach. Discretization of the governing equations is based on central differencing and second-order Euler backward differencing for the spatial and temporal derivatives, respectively. To resolve the transient interaction between the jet and the main-flow boundary layer, a temporal resolution is chosen so that the jet flow takes about 10 timesteps to penetrate a distance equivalent to the displacement thickness of the test-surface boundary layer at the jet orifice, resulting in a timestep size of $\Delta t = 7 \times 10^{-6}$ s. The discretized equations are converged through an algebraic multigrid scheme within eight inner-loop iterations per timestep, reducing the root-mean-square residual of the governing equations by five orders of magnitude to less than 10^{-6}. Approximately 20,000 timesteps are required for the laminar test-surface boundary layer to reach a steady state, after which the vertical jet is impulsively turned on for 8.65 ms—which corresponds to 1236 timesteps—and then impulsively turned off, after which the simulation is then continued for 6400 more timesteps.

RESULTS AND DISCUSSION

In the present discussion of the simulation results, streamwise and spanwise spatial coordinates are normalized

Table 1. Flow conditions and numerical details of the simulations.

	Non-accelerating case	Accelerating case
U_0	4.0 m/s	4.0 m/s
$Re_L = U_0 L/\nu$	143,800	143,800
δ_{xjet}	3.06 mm	2.58 mm
$Re_{\delta_{xjet}}$	800	675
$\Delta\tau = \Delta t U_0/\delta_{xjet}$	9.2×10^{-3}	10.8×10^{-3}
θ	-0.2°	5.6°

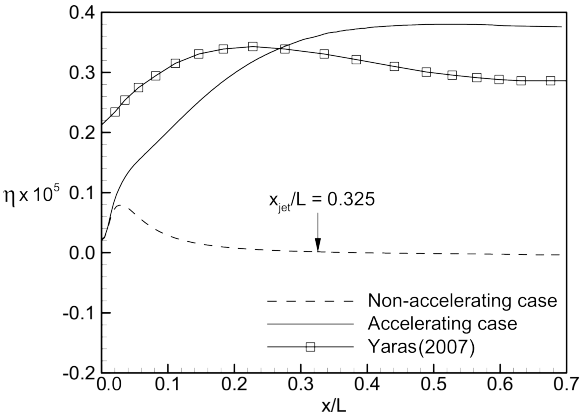

Figure 2. Streamwise distribution of freestream acceleration parameter in the undisturbed main flow.

by the test-surface length L and the wall-normal coordinate is normalized by the 99% boundary-layer thickness of the laminar boundary layer at the center of the jet orifice in the absence of jet flow, denoted by δ_{xjet}. Velocities are normalized by the inlet velocity U_0 and time is normalized by the ratio δ_{xjet}/U_0, which approximates the time required for the freestream fluid to travel a distance equal to one local boundary-layer thickness; for brevity, the normalized time is denoted by τ, and $\tau = 0$ is defined as the instant when the jet is turned off. The values of these parameters for the two simulated cases are given in Table 1.

Figure 2 plots the distribution of the freestream acceleration parameter, $\eta = \nu/U_e^2 dU_e/dx$, where U_e is the local boundary-layer edge velocity. The acceleration parameter downstream of the jet is nominally zero in the non-accelerating case and exceeds $\eta = 3.5\times10^{-6}$ in the accelerating case, which is beyond the critical value required for a turbulent boundary layer to relaminarize (e.g. Escudier et al., 1998). This level of freestream acceleration was chosen with the expectation that the coherent flow structures in the triggered spot would become more organized and thus allow for easier analysis of their spatial and temporal development. Given the strong stabilizing influence of freestream acceleration, the triggering jet needed a relatively large velocity ($v_{jet}/U_0 = 11$) in order to create a turbulent spot.

The numerical approach of the present study is validated by comparing the internal structure of the spot in the accelerating case with measurements of Yaras (2007), which Figure 2 shows to have similar freestream acceleration levels. Figure 3 plots contours of perturbation velocity $\widetilde{u}$ in a spanwise/wall-normal plane that intersects the simulated and measured spots; to enhance the detail, only half the width of the spot is shown in the figure. The perturbation velocity $\widetilde{u}$ is defined in the measurements as the ensemble-averaged velocity, averaged over 75 spot recordings, minus the undisturbed local boundary-layer flow, and in the simulations as the instantaneous velocity minus the undisturbed local boundary-layer flow. The spanwise coordinate is normalized by the spot half-width, s_{spot}, following Sankaran and Antonia (1988) to achieve consistent scaling of the coherent flow structures within both spots. In the present study, the edge of the spot is defined as the furthest spanwise location where the streamwise perturbation velocity exceeds $0.02U_0$. Figure 3 shows that the simulated spot contains the same number of high- and low-velocity streamwise streaks and similar streak amplitudes as the measured spot. The spanwise spacing of the streaks is $\overline{\lambda^+}$ = 250 and 180 wall units for the measured and simulated spots, respectively, where the friction velocity is calculated on the basis of the local wall shear stress in the undisturbed laminar boundary layer. The spanwise edges of both spots are terminated by velocity-deficit regions, in agreement with flow visualizations of Gad-El-Hak et al. (1981), and both spots show low-velocity streaks farther from the wall than high-velocity streaks. These qualitative similarities in the internal structure of the measured and simulated spots occur despite differences in the freestream turbulence intensity (negligible in the simulations, but nearly 1.0% of the local freestream in the measurements) and the shape of the jet orifice (square in the simulations but round in the experiment). This suggests that the numerical method employed in the present study is adequate for in-depth analysis of the mechanisms responsible for the growth of coherent flow structures in the simulated turbulent spots.

The growth of coherent flow structures within the spot begins with the creation of vortices in the test-surface boundary layer by the triggering jet. As described above, a high jet velocity is required to trigger a spot, and the high-momentum jet fluid penetrates through the test-surface boundary layer into the freestream. The interaction between the jet and test-surface boundary layer creates vortical structures that resemble those occurring in the well-documented transverse-jet flow (e.g. Fric and Roshko, 1994). The development of these structures is the subject of an accompanying study, although it suffices to note that a sequence of hairpin vortices are created within the test-surface boundary layer immediately downstream of the jet orifice. Figure 4 visualizes these hairpin vortices in the accelerating case shortly after the jet is turned off (τ = 8.0) through iso-contours of the second-invariant of the velocity gradient tensor normalized by U_0/δ_{xjet}, denoted by Q. The iso-contours are coloured by y/δ_{xjet} to aid in comparing the relative heights of each structure. The flow structure labeled A is a hairpin vortex that was formed while the jet was on and was subsequently convected downstream; structure B is a hairpin vortex that straddles the inside leg of A; and structure C is a hairpin vortex that straddles the inside leg of B. Analysis of previous timesteps reveals that B is created through the reorientation of boundary-layer vorticity upstream of A, indicating that A creates a locally-unstable flow envi-

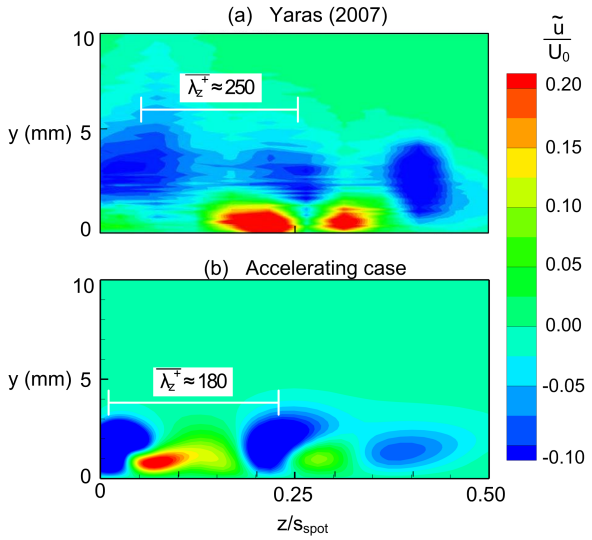

Figure 3. Comparison between (a) spot measured by Yaras (2007) and (b) spot simulated in the accelerating case. Contours show the streamwise component of the perturbation velocity, $\widetilde{u}/U_0$.

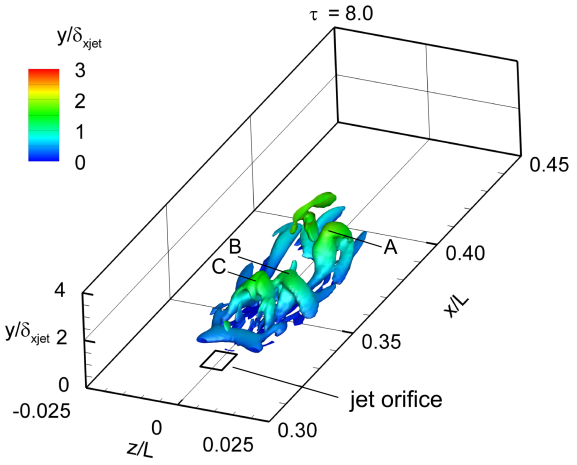

Figure 4. Hairpin vortices downstream of the jet orifice in the accelerating case at τ = 8.0, visualized through isocontours of $Q = 10$ coloured by y/δ_{xjet}.

ronment that allows B to form. The observation that B and C both straddle the inside leg of their parent vortex may indicate that they are created following the mechanism proposed by Schröder and Kompenhans (2004), in which a shear-layer instability in the x-z plane leads to the roll-up of wall-normal vorticity into arch-shaped vortices.

Figure 5 follows the spatial and temporal development of the coherent flow structures triggered by the jet as they convect through the test-surface boundary layer. The dashed line surrounding the spot at $\tau = 10$ aids in distinguishing which structures are contained within the region of perturbed flow that collectively make up the turbulent spot. The large spanwise-oriented structure that is located above the dashed line near the trailing edge of the spot in both the accelerating and non-accelerating cases is the "horseshoe" vortex that is created when boundary-layer vorticity separates upstream of the jet and then wraps around the ejected fluid (e.g. Fric and Roshko, 1994). Once the jet is turned off, this vortex convects downstream and is gradually dissipated. The red-coloured vortices above the spot are remnants of freestream vortices created by the jet. Their colour suggests that these structures are located sufficiently far into the freestream that they should not affect the growth of flow structures within the spot. In the accelerating case in Figure 5a, the hairpin vortices observed in Figure 4 are still visible within the spot at $\tau = 10$ and a third hairpin vortex has started to form, labeled A, straddling the outside leg (i.e. farther from the spot centerline) of the farthest-downstream hairpin vortex. However, by $\tau = 20$, A has become much smaller and no longer has a distinct hairpin shape, and by $\tau = 30$, A has disappeared completely. In addition, several streamwise-oriented vortices that appear near the spanwise edges of the spot at $\tau = 20$, labeled B, have become much smaller and weaker by $\tau = 30$. The diminishing strength of the vortical structures in the spot indicates that the strong freestream acceleration is stabilizing the flow and dissipating the coherent flow structures, hindering the spot's spatial growth as it convects downstream.

In contrast, the non-accelerating case illustrated in Figure 5b shows that coherent flow structures continue to develop as they are convected downstream. Several of these vortical structures are visible at $\tau = 10$: a primary pair of hairpin-shaped vortices near $x/L = 0.44$, labeled A, a secondary pair of hairpin vortices near x/L = 0.42, labeled B, which straddle the outside legs of the vortices in A, and several elongated streamwise vortices between x/L = 0.36 - 0.40 that are almost evenly-spaced in the spanwise direction. As the spot convects downstream, structures A and B are stretched in the streamwise direction—nearly doubling their streamwise length between τ = 10 and τ = 30—and thereby contribute to the longitudinal growth of the spot. By τ = 20, two pairs of hairpin vortices become visible near the trailing edge of the spot. The vortices belonging to the first pair, labeled C, are located near x/L = 0.36 and $z/L = \pm$ 0.005. Each vortex in C straddles one of the elongated streamwise vortices that are visible between x/L = 0.36 - 0.40. The vortices belonging to the second pair, labeled D, are created downstream and to the outside of C, near x/L = 0.38 and $z/L = \pm$ 0.020. Each vortex in D straddles a streamwise vortex that forms near the spanwise edge of the turbulent spot. By τ = 30, the heads of C and D have become larger, their shapes are more clearly defined, and their legs are more widely spaced. By τ = 35 (not shown), C and D have been stretched in the streamwise direction to about three times their initial length, their spanwise extent has nearly doubled, and a third pair of hairpin vortices has formed downstream of D. The analysis of the spot is stopped at τ = 35, beyond which the spot is too close to the outflow boundary to be sure that the flow structures are not being artificially affected by the outflow boundary condition.

The trends visible in Figure 5 indicates that the generation of hairpin vortices near the trailing edge of the spot in the non-accelerating case is primarily responsible for the spot's lateral growth. The pairs of hairpin vortices near the trailing edge are consistently created downstream and to the outside of a previously-formed pair and the vortices belonging to a secondary pair consistently straddle a streamwise vortex

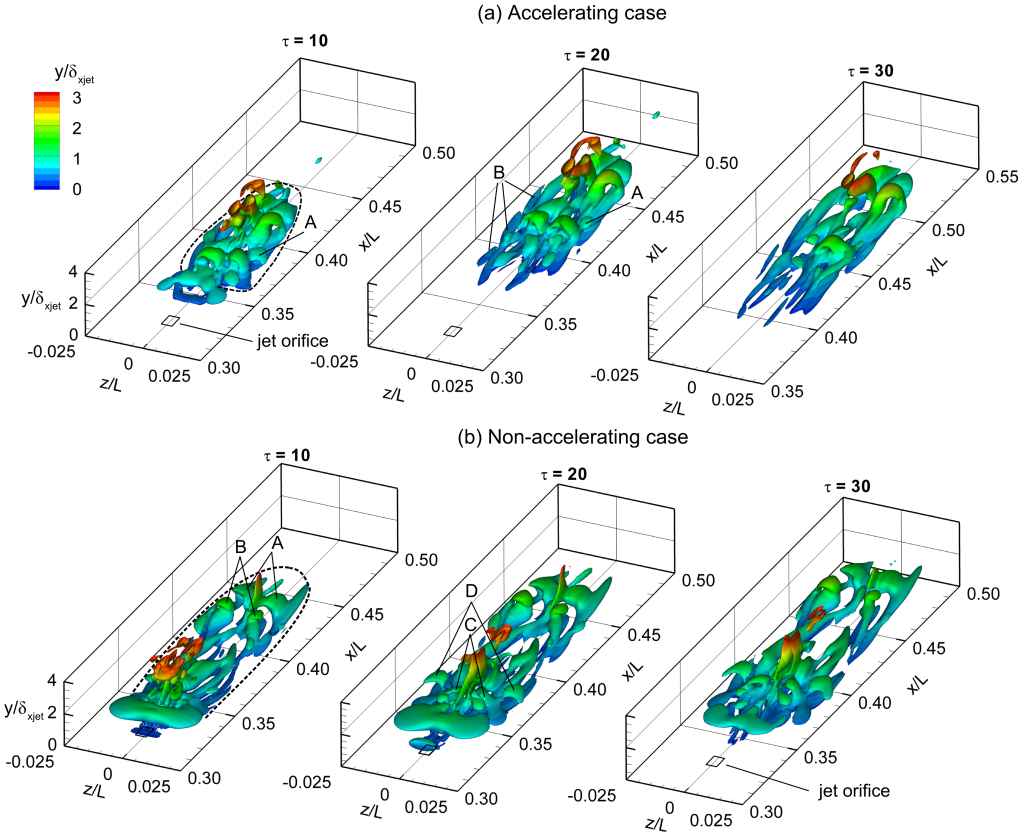

Figure 5. Growth of hairpin vortices in the (a) accelerating and (b) non-accelerating cases visualized through iso-contours of $Q = 10$ coloured by y/δ_{xjet}.

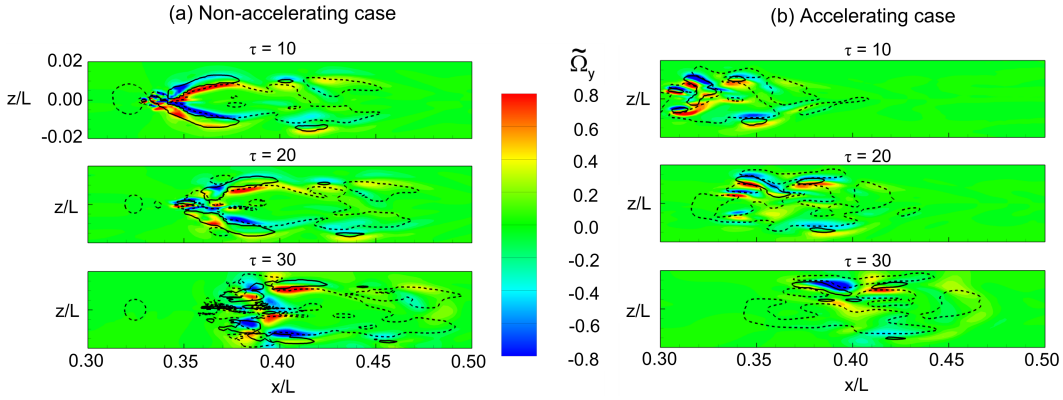

Figure 6. Flood plots of $\widetilde{\Omega}_y$ on a plane at $y/\delta_{xjet} = 0.50$ for the (a) non-accelerating and (b) accelerating cases. Solid and dashed lines correspond to Q2 and Q4 motions, respectively. The z axis labels apply to all frames.

that is formed at the spanwise edge of the spot. Considering that this streamwise vortex is located at the far edge of the spot, it is possible that it is the result of destabilization of the laminar flow near the edge of the spot. To assess this possibility, Figure 6 plots contour flood-plots of the wall-normal component of the perturbation vorticity (the curl of the perturbation velocity described above) normalized by U_0/δ_{xjet}, denoted $\widetilde{\Omega}_y$, and contour lines corresponding to the loci of upwash and downwash motions (denoted as Q2 and Q4, respectively) in an x-z plane at $y/\delta_{xjet} = 0.50$. Q2 motions—which bring low-momentum fluid away from the wall and thus destabilize the boundary layer—are plotted with a solid line, while Q4 motions—which bring high-momentum fluid towards the wall—are plotted with a dashed line. In the non-accelerating case at $\tau = 10$, relatively-uniform regions of $\widetilde{\Omega}_y$ occur near the trailing edge of the spot, which are consistent with the shear layers generated between a low- and high-velocity streak. By $\tau = 20$, instability of this shear layer has started to produce a streamwise grouping of $\widetilde{\Omega}_y$ into several wall-normal-oriented vortices. The sense of the wall-normal-oriented vortices is

such that, as the vortices nearer the spot leading edge are tilted in the streamwise direction by the main shear, they form streamwise vortices that induce upwash in the flow regions just outside the spot perimeter, generating the regions of Q2 motion observed in Figure 6 along the spanwise sides of the spot near the trailing edge. The destabilized flow allows the wall-normal-oriented vortices closer to the spot trailing edge to form hairpin vortices straddling the streamwise vortices. As the spot convects downstream, the region of Q2 motion near the trailing edge becomes less organized as the growing vortical structures within the spot makes the internal flow less orderly, and by $\tau = 30$, the region of Q2 motion has broken into small localized packets near the trailing edge of the spot. Regions of Q2 motion in the accelerating case, shown in Figure 6b, are very small and are observed only in close proximity to the embedded hairpin vortices. Apparently, the strongly-stabilized environment caused by the freestream acceleration prevents the vortical structures from inducing strong wall-normal motions within the spot, and due to the relative absence of Q2 motions in the accelerating case, fewer coherent flow structures develop. These observations suggests that the hairpin vortices near the trailing edge of the spot are predominantly created through an instability of the wall-normal-vorticity shear layer in the manner described by Schröder and Kompenhans (2004). This is consistent with the observations in Figures 4 and 5 of hairpin vortices consistently straddling the legs of parent vortices.

CONCLUSIONS

The growth of coherent flow structures in an artificially-triggered turbulent spot was studied through direct numerical simulations with non-accelerating and strongly-accelerating freestream conditions. Turbulent spots are triggered by a pulsed jet ejected transversely through a square orifice in the test surface. Favorable agreement between the spot in the accelerating case and that measured by Yaras (2007) is obtained in the size, spacing, and amplitude of low- and high-velocity streaks. In the accelerating case, a primary hairpin-shaped vortex created by the jet induces the formation of two upstream hairpin vortices, each straddling the inside leg of the previously-formed vortex. Due to the stabilizing effect of the freestream acceleration, no further growth of coherent flow structures occurs, and the vortices are gradually dissipated. In the non-accelerating case, two pairs of hairpin vortices develop near the leading edge of the spot and three pairs develop in sequence near the trailing edge. The trailing-edge vortices are consistently created downstream and to the outside of the previously-formed vortex pairs, and the secondary vortices consistently straddle a streamwise vortex created near the spanwise edge of the spot. Instability of the wall-normal-vorticity shear layer created between high- and low-velocity streaks near the edge of the spot forms several wall-normal-oriented vortices. Those nearer the spot leading edge are reoriented in the streamwise direction by the mean shear, forming the streamwise vortices and inducing upwash velocities just outside the spot perimeter. Preliminary observations suggest that the destabilized flow allows the wall-normal-oriented vortices closer to the spot trailing edge to form hairpin vortices straddling the streamwise vortices.

REFERENCES

Chong, T. P. and Zhong, S. (2003), "Development of Turbulent Wedges in Favourable Pressure Gradients", *AIAA Paper no. 2003-4245*.

Emmons, H. W. (1951), "The Laminar-Turbulent Transition in a Boundary Layer-Part 1", *Journal of Aeronautical Sciences*, Vol. 18, pp. 490–498.

Escudier, M. P., Abdel-Hameed, A., Johnson, M. W. and Sutcliffe, C. J. (1998), "Laminarisation and Re-transition of a Turbulent Boundary Layer Subjected to Favourable Pressure Gradient", *Experiments in Fluids*, Vol. 26, pp. 491–502.

Fric, T. F. and Roshko, A. (1994), "Vortical Structure in the Wake of a Transverse Jet", *Journal of Fluid Mechanics*, Vol. 279, pp. 1–47.

Gad-El-Hak, M., Blackwelder, R. F. and Riley, J. J. (1981), "On the Growth of Turbulent Regions in Laminar Boundary Layers", *Journal of Fluid Mechanics*, Vol. 110, pp. 73–95.

Guo, H., Lian, Q. X., Li, Y. and Wang, H. W. (2004), "A Visual Study on Complex Flow Structures and Flow Breakdown in a Boundary Layer Transition", *Experiments in Fluids*, Vol. 37, pp. 311–322.

Makita, H. and Nishizawa, A. (2001), "Characteristics of Internal Vortical Structures in a Merged Turbulent Spot", *Journal of Turbulence*, Vol. 2, p. 012.

Perry, A. E., Lim, T. T. and Teh, E. W. (1981), "A Visual Study of Turbulent Spots", *Journal of Fluid Mechanics*, Vol. 104, pp. 387–405.

Sankaran, R. and Antonia, R. A. (1988), "Influence of a Favourable Pressure Gradient on the Growth of a Turbulent Spot", *AIAA Journal*, Vol. 26, pp. 885–887.

Schröder, A., Geisler, R., Elsinga, G. E., Scarano, F. and Dierksheide, U. (2008), "Investigation of a Turbulent Spot and a Tripped Turbulent Boundary Layer Flow Using Time-Resolved Tomographic PIV", *Experiments in Fluids*, Vol. 44, pp. 305–316.

Schröder, A. and Kompenhans, J. (2004), "Investigation of a Turbulent Spot Using Multi-Plane Stereo Particle Image Velocimetry", *Experiments in Fluids*, Vol. 36, pp. 82–90.

Singer, B. A. (1996), "Characteristics of a Young Turbulent Spot", *Physics of Fluids*, Vol. 8, pp. 509–521.

Singer, B. A. and Joslin, R. D. (1994), "Metamorphosis of a Hairpin Vortex into a Young Turbulent Spot", *Physics of Fluids*, Vol. 6, pp. 3724–3736.

Smith, C. R., Walker, J. D. A., Haidari, A. H. and Sobrun, U. (1991), "On the Dynamics of Near-Wall Turbulence", *Philosophical Transactions: Physical Sciences and Engineering*, Vol. 336, pp. 131–175.

Strand, J. S. and Goldstein, D. B. (2011), "Direct Numerical Simulations of Riblets to Constrain the Growth of Turbulent Spots", *Journal of Fluid Mechanics*, Vol. 668, pp. 267–292.

Wygnanski, I., Sokolov, M. and Friedman, D. (1976), "On a Turbulent 'Spot' in a Laminar Boundary Layer", *Journal of Fluid Mechanics*, Vol. 78, pp. 785–819.

Yaras, M. I. (2007), "An Experimental Study of Artificially-Generated Turbulent Spots Under Strong Favorable Pressure Gradients and Freestream Turbulence", *Journal of Fluids Engineering*, Vol. 129, pp. 563–572.